Estimation from PET data of transient changes in dopamine concentration induced by alcohol: support for a non-parametric signal estimation method

2008 Phys. Med. Biol. 53 1353

(http://iopscience.iop.org/0031-9155/53/5/012)

Phys. Med. Biol. **53** (2008) 1353–1367 doi:10.1088/0031-9155/53/5/012

Estimation from PET data of transient changes in dopamine concentration induced by alcohol: support for a non-parametric signal estimation method

C C Constantinescu[1,3], K K Yoder[1], D A Kareken[2], C A Bouman[3], S J O'Connor[4], M D Normandin[1,3] and E D Morris[1,3,4,5]

[1] Department of Radiology, Indiana University School of Medicine, Indianapolis, IN, USA
[2] Department of Neurology, Indiana University School of Medicine, Indianapolis, IN, USA
[3] Weldon School of Biomedical Engineering, Purdue University, West Lafayette, IN, USA
[4] Department of Psychiatry, Indiana University School of Medicine, Indianapolis, IN, USA
[5] Department of Biomedical Engineering, Indiana University-Purdue University at Indianapolis, Indianapolis, IN, USA

E-mail: emorris@iupui.edu

Received 23 July 2007, in final form 7 January 2008
Published 14 February 2008
Online at stacks.iop.org/PMB/53/1353

Abstract

We previously developed a model-independent technique (*non-parametric ntPET*) for extracting the transient changes in neurotransmitter concentration from paired (rest & activation) PET studies with a receptor ligand. To provide support for our method, we introduced three hypotheses of validation based on work by Endres and Carson (1998 *J. Cereb. Blood Flow Metab.* **18** 1196–210) and Yoder *et al* (2004 *J. Nucl. Med.* **45** 903–11), and tested them on experimental data. All three hypotheses describe relationships between the estimated free (synaptic) dopamine curves ($F^{DA}(t)$) and the change in binding potential (ΔBP). The veracity of the $F^{DA}(t)$ curves recovered by nonparametric ntPET is supported when the data adhere to the following hypothesized behaviors: (1) ΔBP should decline with increasing DA peak time, (2) ΔBP should increase as the strength of the temporal correlation between $F^{DA}(t)$ and the free raclopride ($F^{RAC}(t)$) curve increases, (3) ΔBP should decline linearly with the effective weighted availability of the receptor sites. We analyzed regional brain data from 8 healthy subjects who received two [^{11}C]raclopride scans: one at rest, and one during which unanticipated IV alcohol was administered to stimulate dopamine release. For several striatal regions, nonparametric ntPET was applied to recover $F^{DA}(t)$, and binding potential values were determined. Kendall rank-correlation analysis confirmed that the $F^{DA}(t)$ data followed the expected trends for all three validation hypotheses. Our findings lend credence to our model-independent estimates of $F^{DA}(t)$. Application of nonparametric ntPET may yield important insights into how alterations in timing of dopaminergic neurotransmission are involved in the pathologies of addiction and other psychiatric disorders.

1. Introduction

The change in binding potential (ΔBP) between neuroreceptor PET scans under different conditions is often used to quantify the change in receptor occupancy caused by a change in neurotransmitter concentration. However, the binding potential (BP) is a complex integral measure of ligand binding over an entire study whose value reflects a nonlinear interplay of tracer kinetics and endogenous neurotransmitter. We have demonstrated previously that change in BP as a quantitative measure of neurotransmitter release is confounded by neurotransmitter timing (Yoder *et al* 2004). That is, combinations of neurotransmitter timing can occur whereby the lesser release of neurotransmitter actually produces greater ΔBP.

We have recently developed a non-parametric method to extract the timing of the change in neurotransmitter level (Constantinescu *et al* 2007). The method is based on singular value decomposition of PET signals from two scans: rest (neurotransmitter at baseline) and activation (neurotransmitter changing). The method is now referred to as *non-parametric ntPET* in order to distinguish it from an original parametric approach to the same problem developed in our lab, and entitled *ntPET* (neurotransmitter PET) (Morris *et al* 2005). We have tested the *non-parametric ntPET* extensively with simulated [11C]raclopride (RAC) and dopamine (DA) kinetics. We have also shown preliminary agreement between *non-parametric ntPET* and *ntPET* using experimental data. The non-parametric method can locate peak(s) of increases in DA concentration in time. Based on simulations of dynamic data sets that were binned into one-minute time frames, the accuracy of DA peak time localization was shown to be 1–2 min (Constantinescu *et al* 2007).

Previous work has produced theoretical relationships between ΔBP and the kinetics of both the tracer and the neurotransmitter during activation (Endres and Carson 1998, Yoder *et al* 2004). The linear-system theory behind *non-parametric ntPET* is separate and independent of compartmental model theory that led to the Endres and Carson result. In the present study, we sought to further validate the *non-parametric ntPET* method by assessing whether the extracted DA signals satisfied previously demonstrated relationships between measured ΔBP and free DA concentration. Specifically, we tested three hypotheses based on the established relationships: (1) ΔBP decreases with increase in the measured peak time of DA elevation, (2) ΔBP increases with an increase in the correlation in time between free RAC and free DA (3) ΔBP declines with an increase in the previously introduced (Yoder *et al* 2004), effective weighted availability (EWA) of receptor sites. Relationships 1 and 3, above, have been introduced and proven with simulated data in previous work by (Yoder *et al* 2004) and (Morris and Yoder 2007). In section 2.3 we offer theoretical arguments for why we expect relationship 2 to be true. In addition, each hypothesis is first shown to be true using simulated data. Finally, validation is carried out by testing each hypothesis on real PET data. The real data were collected from 8 human subjects who were scanned with [11C]raclopride once at rest, and once during a pharmacologic challenge to provoke striatal DA release (i.e. a transient elevation in synaptic DA).

2. Theory

2.1. Non-parametric ntPET

The non-parametric method for the extraction of free DA ($F^{\mathrm{DA}}(t)$) signals has been described in detail in Constantinescu *et al* (2007). In brief, the PET signals (PET curves in molar concentration units) from each scan were collected in $N \times M$ matrices, with M being the number of signals and N the number of samples. For the present study, the signals from

alcohol scans are called ETOH signals. The signals from the rest scan are called REST signals.

(1) A singular value decomposition (SVD) is applied to the PET signals in order to define a subspace that best spans the rest condition.
(2) The contribution of the rest state to the activated state is 'subtracted' from the ETOH signals by subtracting the projection of the ETOH signals onto the REST subspace defined in Step (1). The resulting signals are called *difference* signals.
(3) A second SVD is applied to the difference signals, and only the most significant components of activation are retained in what we term the *activation* signals.
(4) Finally, a specially designed minimum mean square error (MMSE) filter, trained on simulated RAC data, is applied to the activation signals to yield the estimated free DA signals, $\hat{F}^{\mathrm{DA}}(t)$.

2.2. *Change in binding potential and effective weighted availability*

Endres and Carson derived a theoretical expression for the percent change in total distribution volume (ΔV) of a receptor tracer between REST and ETOH studies (Endres and Carson 1998). The ensuing relationships apply to any displaceable radioligand in competition with an endogenous neurotransmitter. In this work, we deal with RAC and DA so, without loss of generality, we label variables pertaining to neurotransmitter as 'DA' and those pertaining to tracer as 'RAC'.

If one assumes a two-tissue compartmental model to describe the bolus neuroreceptor tracer delivery and binding, the time-varying distribution volume, $V(t)$, of RAC in the presence of a competitor DA, is given by

$$V(t) = \frac{K_1}{k_2}\left(1 + \frac{(k_{\mathrm{on}} B_{\mathrm{avail}}/k_{\mathrm{off}})}{\left(1 + F^{\mathrm{DA}}(t)\big/K_d^{\mathrm{DA}}\right)}\right) \tag{1}$$

where $F^{\mathrm{DA}}(t)$ is the time-varying concentration of free DA, K_d^{DA} is the affinity constant of the endogenous DA and B_{avail} is the concentration of available receptor sites at steady state (Innis *et al* 2007). k_{on} and k_{off} are the association and dissociation rates of the tracer. K_1 and k_2, are the tracer influx/efflux rate constants between the plasma and the free tracer compartment. $V(t)$ is time dependent because of the presence of time-varying neurotransmitter concentration. According to Endres and Carson (1998), the fractional change in total distribution volume between the REST and ETOH scans will be

$$\Delta V = \left(\frac{\mathrm{BP}_{\mathrm{ND}}^{(\mathrm{REST})}}{1 + \mathrm{BP}_{\mathrm{ND}}^{(\mathrm{REST})}}\right)\left\{1 - \frac{1}{BP_{\mathrm{ND}}^{(\mathrm{REST})}}\int_0^\infty \left[\frac{F^{\mathrm{RAC}}(t)}{\int_0^\infty F^{\mathrm{RAC}}(t)\,\mathrm{d}t}\right]\left[\frac{(k_{\mathrm{on}} B_{\mathrm{avail}}/k_{\mathrm{off}})}{\left(1 + F^{\mathrm{DA}}(t)\big/K_d^{\mathrm{DA}}\right)}\right]\mathrm{d}t\right\}. \tag{2}$$

$F^{\mathrm{RAC}}(t)$ is the molar concentration of free RAC in the tissue during ETOH scan. $\mathrm{BP}_{\mathrm{ND}}^{(\mathrm{REST})}$ is the binding potential resulting from the REST scan. The subscript 'ND' refers to nondisplaceable tracer. $\mathrm{BP}_{\mathrm{ND}}$ is equivalent to the equilibrium ratio of specifically bound to nondisplaceable tracer in tissue (Innis *et al* 2007). In practice, binding potential (BP) is often used instead of V since it is a more direct indicator of specific binding. Based on their definitions, ΔBP and ΔV can be related by $\Delta\mathrm{BP} = \left(\frac{1+\mathrm{BP}_{\mathrm{ND}}^{(\mathrm{REST})}}{\mathrm{BP}_{\mathrm{ND}}^{(\mathrm{REST})}}\right)\Delta V$.

Equation (2) has been simplified (Yoder *et al* 2004) and expressed as a linear equation for ΔBP as follows

$$\Delta\mathrm{BP} = 1 - m \cdot \mathrm{EWA} \tag{3}$$

where

$$\text{EWA} = \int_0^\infty \frac{F^{\text{RAC}}(t)}{K_d^{\text{DA}} + F^{\text{DA}}(t)}\,\text{d}t \qquad \text{and} \qquad m = \left(\frac{K_d^{\text{DA}}}{\text{BP}_{\text{ND}}^{(\text{REST})}}\right) \cdot \left(\frac{k_{\text{on}} B_{\text{avail}}}{k_{\text{off}}}\right) \Big/ \int_0^\infty F^{\text{RAC}}(t)\,\text{d}t.$$

The effective weighted availability (EWA) is an interaction term between the free RAC and free DA during the activation scan. As the EWA of receptor sites is driven to 0 by free DA, change in binding potential must go to a maximum (i.e., ΔBP->1). The slope term, *m,* is a constant provided $\int_0^\infty F^{\text{RAC}}(t)\,\text{d}t$ is constant.

2.3. Hypotheses testing

To assess the plausibility of the $\hat{F}^{\text{DA}}(t)$ signals that have been extracted with *non-parametric ntPET* ('^' indicates estimated), we have tested three expected trends that emerge from equation (3) or from its components.

(1) *ΔBP decreases with increasing peak time of the $\hat{F}^{\text{DA}}(t)$.* It was shown in Yoder *et al* (2004) via simulations that, for elevations in DA that start after tracer injection, measured ΔBP is lower for elevations with peak times occurring later in the scan. This can be inferred from the components of the integral in the definition of EWA. The amount of free RAC available to compete with DA for receptor sites decreases over time. For a given RAC curve, a late peak in DA will diminish EWA less than an early peak. Lower EWA will result in higher ΔBP.

(2) *ΔBP increases with increased strength of the correlation in time between $F^{\text{RAC}}(t)$ and $\hat{F}^{\text{DA}}(t)$.* EWA combines the effects on receptor availability of both time-varying free RAC and time-varying free DA. Since the free RAC and the free DA compete for the same receptor sites, $F^{\text{RAC}}(t)$ is also a function of $F^{\text{DA}}(t)$. As the strength of the temporal correlation between $\hat{F}^{\text{DA}}(t)$ and $F^{\text{RAC}}(t)$ increases, that is the peak of F^{DA} occurs closer in time to the peak of RAC, the ratio $F^{\text{RAC}}(t)/\hat{F}^{\text{DA}}(t)$ will be significantly reduced at the peak level and the EWA integral will be minimized. According to equation (3), small EWA yields large ΔBP. The correlation between $\hat{F}^{\text{DA}}(t)$ and $F^{\text{RAC}}(t)$ will be referred to as corr($\hat{F}^{\text{DA}}(t)$, $F^{\text{RAC}}(t)$).

(3) *ΔBP declines linearly with EWA.* This linear relationship emerges directly from equation (3), provided the components of m are constant. Ideally, the plot of ΔBP as a function of EWA should be a line with slope m and intercept 1. For different tracers with different kinetics, the plots of ΔBP versus EWA have been shown to be a collection of lines with different negative slopes all converging at [0, 1]. That is, they make a *fan* shape with a vertex at [0, 1] (see Morris and Yoder (2007)).

3. Methods

3.1. Experimental data acquisition and pre-processing

Eight healthy social drinkers (all caucasians, 5 male, mean age = 23.8 years, SD = 4.03) signed informed consent statements agreeing to participate in the study, which was approved by the Indiana University Institutional Review Board. Each subject underwent three RAC PET scans across two days on an ECAT EXACT HR+ as part of a larger study (Kareken *et al* 2007). For this purpose, we are modeling data only from the REST condition (day 1) and the ETOH (day 2) condition. The injected RAC activity was 14.136 $\pm$ 0.990 mCi, and the specific activity at time of injection was 1.0 $\pm$ 0.3 mCi μmol^{-1}. Briefly, the first scan (REST)

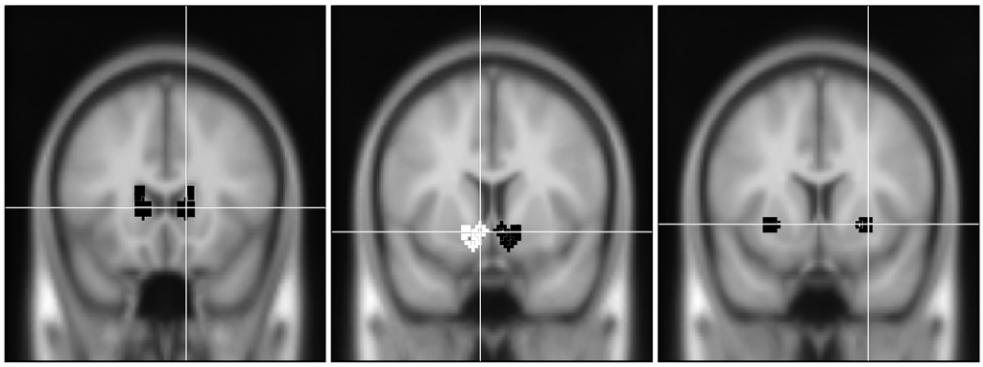

Figure 1. Coronal MR slice containing representative ROI placement for the caudate (4 ROIs shown, left image), nucleus accumbens (NAcc) (6 ROIs shown, center image) and putamen (2 ROIs shown, right image). The rest of the 24 ROIs are not shown. The left NAcc ROIs are shown in white, while the rest of ROIs are shown in black.

was acquired while subjects received a lactated ringer's infusion (eyes open). The second scan (ETOH) was done under the same conditions, except that subjects received an unexpected iv infusion of 6% alcohol in lactated ringer's to target a breath alcohol concentration of 80mg% (Ramchandani *et al* 1999), which was maintained until scan completion. Both lactated ringer's and alcohol infusion started, respectively, 4 min post-RAC injection.

The duration of each dynamic scan was 45 min (10 × 30 s, 40 × 1 min). Images were reconstructed using filtered backprojection with a 5 mm Hanning filter (FWHM was 9 mm at center of FOV). A T1-weighted MR image of each subject was acquired (1.5T GE Echospeed LX scanner). PET images were motion-corrected by co-registration of each frame to an early summed (10 min) PET image using Statistical Parametric Mapping 2 (SPM2) software (http://www.fil.ion.ucl.ac.uk/spm). The summed image was then co-registered to the subject's MR scan, and the resulting transformation matrix was applied to each PET image, individually. The MR image was normalized to the standardized Montreal Neurological Institute (MNI) coordinate system using the SPM2 default normalization parameters. The resulting transformation matrix was applied to the motion-corrected, co-registered PET data. The final interpolated voxel size of the transformed PET images was 2 mm × 2 mm × 2 mm. Twenty-four spherical regions of interest (ROIs) were drawn on three major regions of the striatum: the Nucleus Accumbens (NAcc; 12 ROIs, 268 mm^3 each), the putamen (6 ROIs, 524 mm^3), and the caudate nucleus (6 ROIs, 524 mm^3) (see figure 1). The regions were equally and symmetrically distributed between the two hemispheres of the brain. In addition, two box-shaped ROIs (450 mm^3 each) were placed on the left and right posterior cerebellum. The 26 ROIs were then projected onto the 50 dynamic PET images. Time-activity curves (TACs) were constructed using the average signal in each ROI at each time point. The TACs were decay-corrected and converted to molar concentration via the specific activity of RAC. We refer to the resulting curves in molar units as 'PET signals'. Each PET signal consists of a number of samples, equal to the number of time frames. As established previously (Constantinescu *et al* 2007), the *non-parametric ntPET* method requires data sampled at equally-spaced time intervals. To satisfy this requirement, every two 30-second frames at the beginning of the scan were averaged so that the resulting PET signals each contained 45 × 1 min-samples. In all, we used 26 PET signals (i.e. 26 ROIs = 26 signals) for each condition, REST and ETOH.

3.2. Simulated data

In order to illustrate the ideal behavior represented by each of our three hypotheses, we generated noiseless simulations of striatal RAC PET signals under REST and ETOH conditions. The simulations were performed using the enhanced compartmental model that accounts for the increase of an endogenous neurotransmitter and its competition for available receptor sites with an exogenous tracer (Morris *et al* 1995). All curves were characterized by the same tracer kinetics (i.e., tracer parameters). The RAC kinetic parameters where the same ones used in Yoder *et al* (2004), which were modified values of ones used in Pappata *et al* (2002) and in Endres and Carson (1998). The values were $K_1 = 0.0918$ ml min^{-1} g^{-1}, $k_2 = 0.333$ min^{-1}, $k_{on} = 0.0023$, $B_{max} = 44$ pmol ml^{-1}, $k_{off} = 0.02$. The kinetic parameters used to describe binding of endogenous DA were $k_{on}^{DA} = 25$ ml·pmol^{-1}·min^{-1} and $k_{off}^{DA} = 0.25$ min^{-1} (Fisher *et al* 1995). The F^{DA} curves were simulated as gamma-variate functions as follows:

$$F^{DA}(t) = \text{Basal} + \gamma \cdot (t - d)^{\alpha} \cdot \exp(-\beta(t - d)) \tag{4}$$

where Basal = 100 pmol ml^{-1}, $\alpha = 1$, $\beta = 1.2$ min^{-1}, d = [1, 2, . . . , 10] min, $\gamma = 7000$ pmol ml^{-1}. RAC injection occurs at $t = 0$. The DA parameters were chosen to generate multiple functions that had the same height and shape but different onset times, d, and therefore different peak times relative to RAC injection. An ideal cerebellum curve was also generated using the same parameters as those of striatal simulations, but with k_{on}, Basal and γ equal to 0. The cerebellum serves as a D_2 receptor-free 'reference region' for calculation of BP (Logan *et al* 1996). The TACs from the cerebellum are used in lieu of an arterial input function. The total duration of each simulated scan was 90 min and was made up of 540 acquisition frames (540 × 10 s). In addition, to illustrate the relationship between EWA and ΔBP, we used simulated data generated for a recent publication from our group (Morris and Yoder 2007). The simulations were for 6 different sets of tracer kinetics for five different D_2 receptor ligands: RAC1 (parameters based on Pappata *et al* (2002) and Yoder *et al* (2004)), RAC2 (parameters based on Endres and Carson (1998) and Yoder *et al* (2004)), [11C]N-methyl-spiperone (NMSP) (Eckernas *et al* 1987), [18F]fallypride (Christian *et al* 2004), [18F]fluoro-ethyl spiperone (FESP) (Bahn *et al* 1989) and [11C]FLB 457 (FLB) (Olsson and Farde 2001).

3.3. Data analysis

Using *non-parametric ntPET*, we analyzed the experimental striatal ROI data for all 8 subjects and extracted $\hat{F}^{DA}(t)$ signals from each subject's 24 ROIs. The $\hat{F}^{DA}(t)$ curves estimated by *non-parametric ntPET* typically contained multiple peaks and troughs. Therefore, we applied an objective procedure to identify the overall peak time as follows: each $\hat{F}^{DA}(t)$ signal was convolved (filtered) with a 10-min square kernel in order to identify the 10 min interval during which the integral of the $\hat{F}^{DA}(t)$ signal was maximal. The peak time of each $\hat{F}^{DA}(t)$ was given by the peak time of the convolved signal. The width of the kernel was chosen to be consistent with the MMSE filter size (10 min), originally applied to extract the $\hat{F}^{DA}(t)$ signal (see theory).

Binding potential for each striatal ROI was measured graphically using the Logan plot (Logan *et al* 1996). The difference in binding potential was calculated as $\Delta BP = \left(BP_{ND}^{(REST)} - BP_{ND}^{(ETOH)}\right)/BP_{ND}^{(REST)}$, where $BP_{ND}^{(REST)}$, and $BP_{ND}^{(ETOH)}$ are the BP values from the REST and ETOH TACs, respectively. The right and left cerebellar TACs were used as the input function for right and left striatal ROIs, respectively. To insure linearity of the Logan plots, data from the first 25 min of the scans were excluded.

The Kendall rank-correlation coefficient, τ, was used to test for the following relationships:

(1) the dependence of ΔBP on $\hat{F}^{\mathrm{DA}}(t)$ peak time; specifically, whether ΔBP decreased as the peak time increased;
(2) the dependence of ΔBP on the corr$(\hat{F}^{\mathrm{DA}}(t), F^{\mathrm{RAC}}(t))$; specifically, whether ΔBP increased with increasing corr$(\hat{F}^{\mathrm{DA}}(t), F^{\mathrm{RAC}}(t))$.

Kendall τ (Kendall 1955) measures the degree of correspondence between two rankings, or the strength of association between two variables. We used this measure since it does not require the assumption that the relationship between the variables is linear. Rank-correlations were considered significant at $p < 0.05$. Trend-level (weak) correlations were defined as $0.05 \leq p \leq 0.1$.

Since the true $F^{\mathrm{RAC}}(t)$ was not available from our analysis, we used the cerebellum TAC, $F^{\mathrm{RAC}}_{\mathrm{cereb}}(t)$ from the ETOH scan as an approximation of $F^{\mathrm{RAC}}(t)$ in striatum. The corr$\left(\hat{F}^{\mathrm{DA}}(t), F^{\mathrm{RAC}}_{\mathrm{cereb}}(t)\right)$ was the correlation coefficient of each pair of curves, $\left(\hat{F}^{\mathrm{DA}}(t), F^{\mathrm{RAC}}_{\mathrm{cereb}}(t)\right)$, and was calculated using Matlab function *corrcoeff*.

It has been shown in Constantinescu *et al* (2007) that the absolute scale of $\hat{F}^{\mathrm{DA}}(t)$ signals cannot be recovered. We also do not know the exact value of K_d^{DA} *in vivo*. In order to prevent the denominator of the integrand in the expression of EWA from being dominated by either $\hat{F}^{\mathrm{DA}}(t)$ or K_d^{DA}, we rescaled the $\hat{F}^{\mathrm{DA}}(t)$ signals so that their mean height equaled the value of K_d^{DA}, which we assumed to be 100 nM. In other words, we enforced the condition that, at baseline, DA is 50% bound and 50% free, in line with the assumed basal DA concentration of 100 nM (Fisher *et al* 1995).

The relationship between ΔBP and EWA from the human data was examined visually for consistency with the relationships seen with the simulated data from multiple tracers.

3.4. Identification of areas with alcohol-induced DA increase

In a recent work (Kareken *et al* 2007) our colleagues performed a voxel-wise analysis of the same subjects presented here to identify brain areas with significant changes in BP in response to the ETOH condition. In short, $\mathrm{BP_{ND}}$ images were generated via graphical analysis for each scan (REST and ETOH), for each subject. Voxel-wise statistical analysis (paired *t*-test) of the differences in $\mathrm{BP_{ND}}$ images between REST and ETOH conditions were conducted using SPM2. Relative to REST, the EtOH condition resulted in significantly ($p < 0.005$) decreased $\mathrm{BP_{ND}}$ in the left ventral striatum, which contains the NAcc. The six spherical ROIs placed on the left NAcc covered the voxels of activation. Thus, we refer to these ROIs as the 'alcohol responding' ROIs. The remaining 18 ROIs are considered to be non-responding ROIs (i.e., no significant decrease in BP during IV alcohol). In the present study, we tested each of our three hypotheses on $\hat{F}^{\mathrm{DA}}(t)$ signals estimated from each of the 24 ROIs in each subject. We used the SPM study results as a guide to analyze the alcohol responding and non-responding ROIs separately. It was predicted that $\hat{F}^{\mathrm{DA}}(t)$ curves in the responding regions would satisfy the postulated relationships, while $\hat{F}^{\mathrm{DA}}(t)$ curves recovered from non-responding regions would be primarily a result of noise in the data, and therefore would not display the relationships described above.

4. Results

The $\hat{F}^{\mathrm{DA}}(t)$ signals extracted from both the responding and non-responding ROIs from each of the eight subjects are presented in figure 2. The six $\hat{F}^{\mathrm{DA}}(t)$ signals extracted from the left NAcc ROIs for each subject are shown in figure 3.

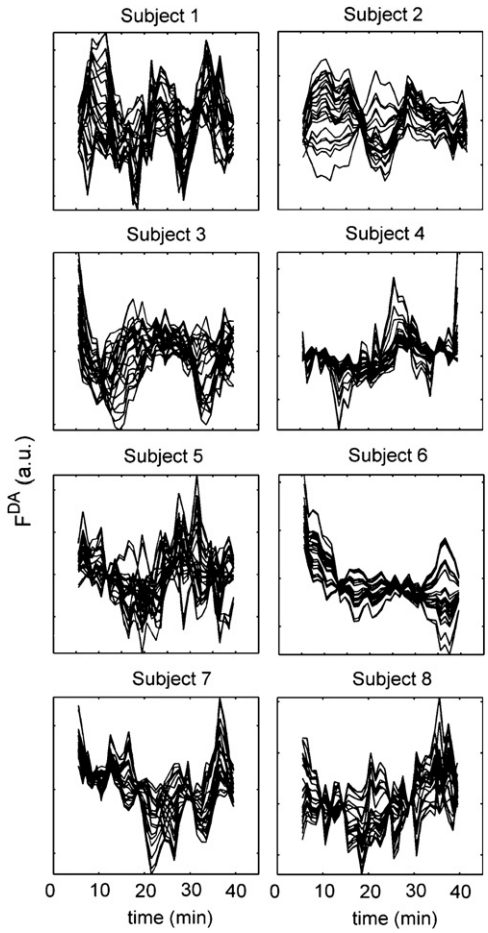

Figure 2. Estimate of alcohol-induced $\hat{F}^{\mathrm{DA}}(t)$ in striatum (in au). Each panel corresponds to a subject and shows signals from 24 different ROIs. The central 35 min of the recovered signals are displayed in the figure.

Simulated data were used to demonstrate the *ideal* behaviors of ΔBP with respect to F^{DA} peak time, corr($F^{\mathrm{DA}}(t)$, $F^{\mathrm{RAC}}(t)$), and EWA, and these data are presented in figure 4. The family of 10 $F^{\mathrm{DA}}(t)$ used to simulate the PET data is shown in figure 4(a). In figure 4(b), ΔBP can be seen to decrease with the increasing F^{DA} peak time. Note that this trend is not linear. The plot in figure 4(c) shows that ΔBP is positively correlated with corr($F^{\mathrm{DA}}(t)$, $F^{\mathrm{RAC}}(t)$). Figure 4(d) reveals linear relationships with negative slopes between ΔBP and EWA, for each of six different tracers, as described previously (Morris and Yoder 2007). The particular slope is a function of the kinetic parameters of the given tracer. All the plotted lines appear to intercept the *y*-axis at [0, 1], the point on the graph that would occur at complete occupancy of all receptors. This condition is not realizable in real experiments or in simulations of transient and short-lived DA perturbations.

Figure 5 shows plots of ΔBP as a function of the peak time of the $\hat{F}^{\mathrm{DA}}(t)$ signals extracted from all the ROIs from all subjects (left panel), from the left NAcc (alcohol-responding) ROIs only (middle), and from non-responding ROIs (right). In all cases, only ROIs with positive ΔBP were considered, because a positive value represents increased DA concentration, and the

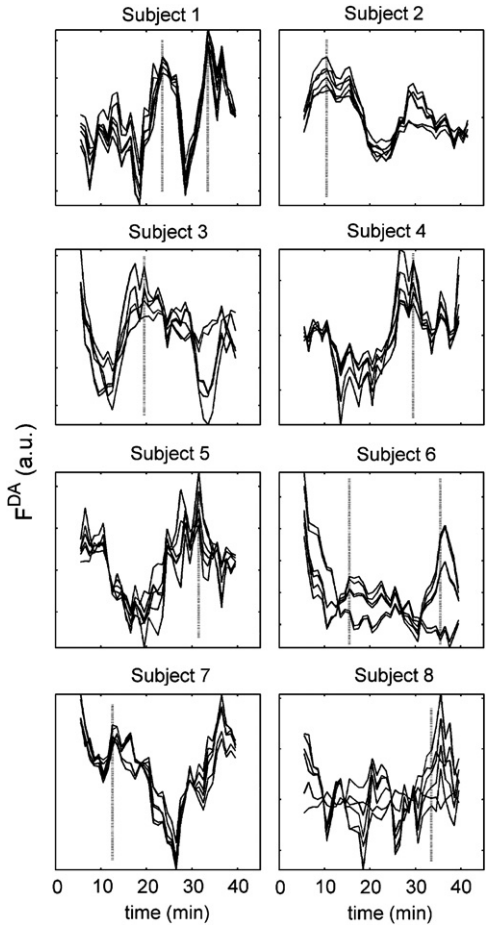

Figure 3. Estimate of alcohol-induced $\hat{F}^{\mathrm{DA}}(t)$ in left NAcc (in au). Each panel corresponds to a subject and shows signals from 6 different ROIs. The central 35 min of the recovered signals are displayed in the figure. The vertical dotted lines indicate the position of the detected peak time.

postulated relationships are defined only for conditions with positive ΔBP. Thus, the number of data points that appear on each plot in figure 5 varies. Error bars for ΔBP are also shown in the plots. The error in ΔBP was estimated using propagation of uncertainties from the errors in $\mathrm{BP}^{(\mathrm{REST})}$ and $\mathrm{BP}^{(\mathrm{ETOH})}$. The error in $\mathrm{BP}^{(\mathrm{REST})}$ was computed based on the inter-subject standard deviation of all measurements of $\mathrm{BP}^{(\mathrm{REST})}$ ($n = 8$) for each respective ROI. The mean error for $\mathrm{BP}^{(\mathrm{ETOH})}$ was assumed equal to that of $\mathrm{BP}^{(\mathrm{REST})}$. When all regions were considered, the rank-correlation between ΔBP and peak time of $\hat{F}^{\mathrm{DA}}(t)$ was not significant ($\tau = -0.0184$, $p = 0.7889$). However, the correlation was significant when only alcohol-responding regions were analyzed ($\tau = -0.2544$, $p = 0.0411$). There was no significant relationship between peak times recovered from non-responding regions and ΔBP ($\tau = 0.0937$, $p = 0.2654$).

Figure 6 shows a plot of ΔBP as a function of the correlations in time between the extracted $\hat{F}^{\mathrm{DA}}(t)$ signals and our approximation of $F^{\mathrm{RAC}}(t)$ (i.e., the cerebellum TACs, $F^{\mathrm{RAC}}_{\mathrm{cereb}}(t)$). As in figure 5, only data with positive ΔBP were considered. When all regions were considered together, there was no significant relationship between of ΔBP and corr($\hat{F}^{\mathrm{DA}}(t)$, $F^{\mathrm{RAC}}_{\mathrm{cereb}}(t)$ ($\tau = 0.1138$, $p = 0.0820$; figure 6(a)). For the responding regions (figure 6(b)), the rank-correlation

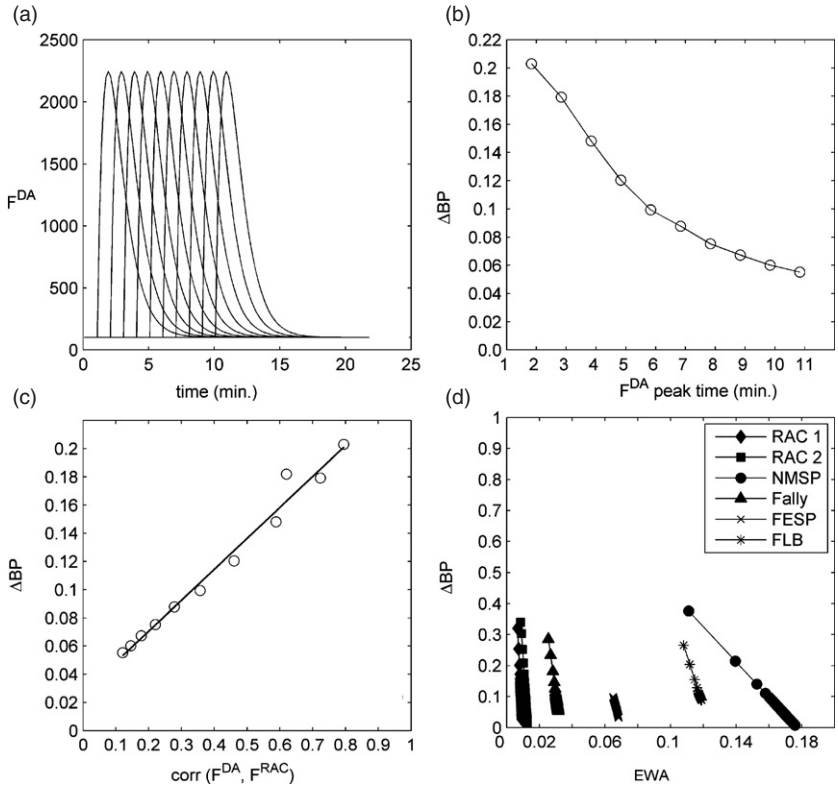

Figure 4. (a) Gamma-variate functions representing F^{DA} responses used in RAC simulations. The curves have onset times $d = [1, 2, \ldots, 10]$ min. (b) ΔBP with respect to the peak of each F^{DA} curve (c) ΔBP with respect to correlation in time between F^{DA} and simulated free tissue RAC, $F^{\mathrm{RAC}}(t)$. (d) Plot of ΔBP as a function of EWA for multiple F^{DA} responses (including those shown in panel (a)) for 6 different tracers. The tracer parameters were taken from the literature.

was significant ($\tau = 0.2437$, $p = 0.0402$), whereas within the non-responding regions (figure 6(c)) no significant relationship between ΔBP and $\mathrm{corr}\left(\hat{F}^{\mathrm{DA}}(t), F^{\mathrm{RAC}}_{\mathrm{cereb}}(t)\right)$ was observed ($\tau = 0.0122$, $p = 0.8826$). Note that in figures 5 and 6 the displayed lines are a best fit to all the points, but the Kendall rank-correlation coefficient does not require a linear relationship.

Figure 7 shows plots of ΔBP as a function of EWA. Again, only ROIs with positive ΔBP were considered. Note the 'fan-like' appearance of the plots, which is consistent with the simulated data in figure 4(d).

5. Discussion

5.1. Dependence of ΔBP on the F^{DA} peak time

As predicted by theory (equation (3)), ΔBP was negatively correlated with the peak time of free DA concentration. Interestingly, the rank-correlation was not significant when all striatal were included in the analysis. The rank-correlation was significant for ROIs from the left Nacc alone, a region which had previously been identified by conventional voxel-wise

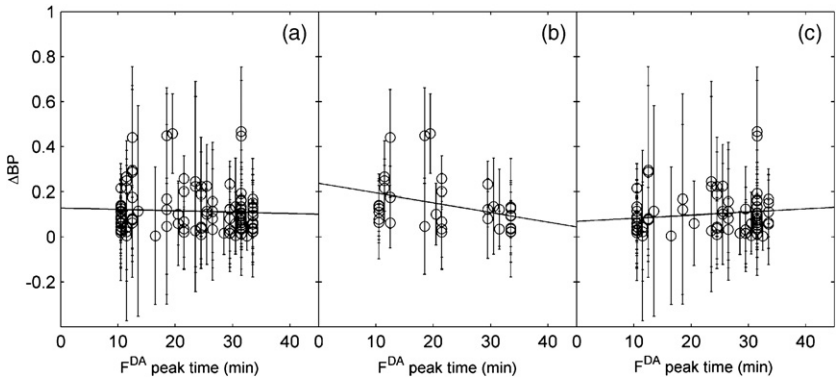

Figure 5. Plot of ΔBP as a function of F^{DA} peak time for (a) all 24 striatal ROIs, (b) 6 ROIs from an area responsive to alcohol (Left NAcc) and (c) 18 ROIs not responsive to alcohol. Data from eight subjects receiving IV alcohol were included. Only data with positive ΔBP were considered. Trend lines are shown as a visual aid only.

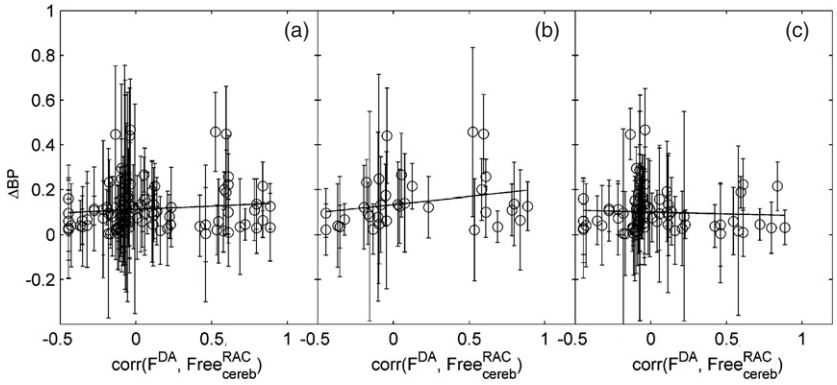

Figure 6. Plot of ΔBP as a function of the correlation in time between F^{DA} and F^{RAC} for (a) all 24 striatal ROIs, (b) 6 ROIs from an area responding to alcohol (Left NAcc) and (c) 18 ROIs not responding to alcohol. Data from eight subjects receiving IV alcohol were included. Only data with positive ΔBP were considered. Trend lines are shown as a visual aid only.

analysis of the same subjects as presenting significant increases in DA concentration (Kareken *et al* 2007). The left NAcc is the site of increased DA concentration in these subjects, which may explain why a significant inverse relationship between ΔBP and $\hat{F}^{\mathrm{DA}}(t)$ peak time was detected only in the left NAcc ROIs. Thus, we interpret $\hat{F}^{\mathrm{DA}}(t)$ signals from all other ROIs as being random signals caused by noise. Observation of the predicted dependence of ΔBP on $\hat{F}^{\mathrm{DA}}(t)$ peak time only in the left NAcc supports the idea that we have extracted bona fide temporal information on DA release for that region.

The estimated peak times span a wide range despite a common start time for alcohol delivery for all subjects (figures 2 and 3). This result could be explained by the fact that the alcohol was infused over an extended period of time, so the stimulus did not occur at a single instant in time. The variability in the response of different subjects may be an inherent characteristic of alcohol.

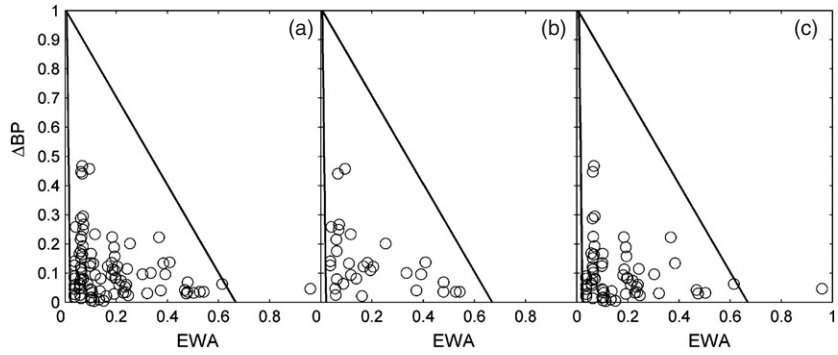

Figure 7. Plot of ΔBP as a function of EWA for in (a) all 24 striatal ROIs, (b) 6 ROIs from an area responding to alcohol (Left NAcc) and (c) 18 ROIs not responding to alcohol. Data from eight subjects receiving IV alcohol were included. Only data with positive ΔBP and EWA were considered. Lines were added strictly as a visual aid.

5.2. Correlation of ΔBP with corr($\hat{F}^{DA}(t)$, $F^{RAC}_{cereb}(t)$)

The second validation test of nonparametric ntPET showed that ΔBP was significantly increased with greater correlation between the $\hat{F}^{DA}(t)$ and $F^{RAC}_{cereb}(t)$ signals in the left NAcc ROIs. When all ROIs were analyzed together or just the non-responding ROIs were analyzed, there were no associations between ΔBP and corr$\left(\hat{F}^{DA}(t), F^{RAC}_{cereb}(t)\right)$. It is important to note that we used the cerebellum curve from the ETOH scan as an approximation to the $F^{RAC}(t)$ curve which cannot be measured directly without a plasma input function. The cerebellum is essentially devoid of DA receptors, and thus, the cerebellum curve is often used as an acceptable approximation of the free RAC curve. However, in the striatum, RAC and endogenous DA compete for the same receptor sites, and as such, the kinetics of free RAC and free DA are coupled. Figure 8 compares a 'true' simulated striatal $F^{RAC}(t)$ with both a simulated and a measured $F^{RAC}_{cereb}(t)$. Transient increases in DA cause bound RAC to dissociate from the receptor sites so $F^{RAC}(t)$ increases transiently during the scan. This can be seen as a short-lived upward inflection in the $F^{RAC}(t)$ curve at about 22 min. There is no corresponding inflection on the cerebellum curves. Thus, the cerebellum is only a poor estimate of striatal $F^{RAC}(t)$, and we might expect that the correlations in time between the striatal $\hat{F}^{DA}(t)$ signals and $F^{RAC}_{cereb}(t)$ would be weak, at best. Although a significant relationship was detected between ΔBP and corr$\left(\hat{F}^{DA}(t), F^{RAC}_{cereb}(t)\right)$ in the left NAcc, we suspect that the strength of this association is slightly underestimated since $F^{RAC}_{cereb}(t)$ is not very faithful to the true $F^{RAC}(t)$.

5.3. ΔBP versus EWA

The third assessment of the free DA signals recovered from nonparametric ntPET yielded a qualitative indication of the dependence of the measured ΔBP on the calculated EWA (figure 7). It can be seen from the data presented in figure 4(d) that under ideal conditions (noiseless data, with limited or no kinetic variability across regions), ΔBP varies linearly with EWA for a given set of kinetic parameters. However, we also note that the integral in the expression of m from equation (3) has limits of 0 and infinity, while in the case of our experimental data we integrated only from 0 to 45 min (the duration of RAC scan). In practice, we cannot integrate from zero to infinity because the PET scan duration is finite. The short integration interval should have limited impact on the linearity between ΔBP and EWA if the DA and RAC concentrations have returned to baseline and zero, respectively, by

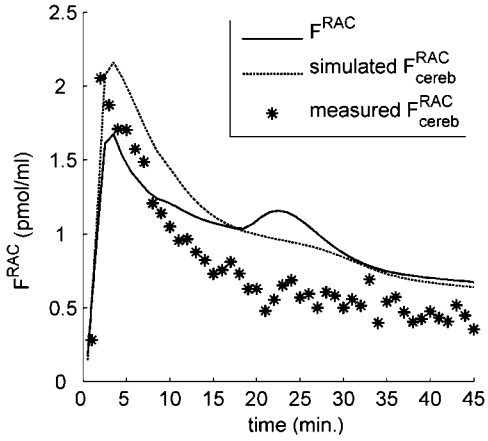

Figure 8. Plot of one simulated free tissue RAC, $F^{\mathrm{RAC}}(t)$ curve (solid curve) with the DA response initiated at 18 min, simulated free RAC in the cerebellum, $F^{\mathrm{RAC}}_{\mathrm{cereb}}(t)$ (dashed curve), and an example of measured PET signal in left cerebellum region from a subject scanned under ETOH condition (stars).

the end of the scan. On the other hand, the integral $\int_0^\infty F^{\mathrm{RAC}}(t)\,\mathrm{d}t$ is a function of PET scan, depending on the injected dose and RAC kinetics, and will vary from subject to subject. The large spread in the slope presented in the plot could be explained in part by considering that data from all subjects was included and thus the slope m varies. Nonetheless, the observation of the 'fan' indicated by the lines on the plots in figure 7 suggests behavior consistent with the theory-based expectations illustrated in figure 4(d).

5.4. Limitations

There are a number of limiting factors that cause the experimental data to depart from the ideal behaviors depicted in figure 4. Timing of the DA response is not the only factor that affects ΔBP. As can be seen in equation (3), ΔBP is a complex measure that is a function of both tracer and neurotransmitter concentrations. A sufficiently large but late F^{DA} peak could generate a larger ΔBP than a smaller peak occurring earlier.

The measurement of ΔBP with a graphical method assumes that the system reaches a pseudo-steady-state during the scan. Due to the presence of time-varying neurotransmitter concentration, this requirement may not fully be satisfied. Because we used a fixed cutoff (25 min) for the Logan plots, the measured $\mathrm{BP_{ND}}$ may not be accurate for those TACs that did not satisfy the pseudo-steady state requirements of the Logan plot, most likely to be invalidated by late DA perturbations.

1 min frames used in this study are not typical for dynamic PET experiments. The short acquisition frames are necessary to achieve good temporal resolution but they may lead to poor counting statistics. Nevertheless, our previous study with realistic noisy simulations indicated that the method performs well with 1-min frames. Luckily, access to list-mode data enables the end-user to reconstruct the PET images with whatever frame time represents best tradeoff scenario between temporal resolution and counting statistics.

5.5. Final remarks

DA signals recovered with nonparametric ntPET from eight human subjects receiving IV alcohol appeared to adhere to three proposed validation hypotheses. These three relationships

were postulated based on the theory of how ΔBP varies with both tracer and neurotransmitter fluctuations.

Our results for left NAcc are consistent with the theory that an unexpected reward (in this case unexpected alcohol) causes an increase in firing of dopaminergic neurons in the striatum (Mirenowicz and Schultz 1994, Schultz *et al* 2000, Pan *et al* 2005). The demonstrated consistency of the estimated F^{DA} signals with the predicted relationships lends support to the utility of our *non-parametric ntPET* method for estimating neurotransmitter behavior from paired bolus PET studies.

Acknowledgments

This work was funded in part by grants from the Whitaker Foundation (RG 02 0126 and TF 04 0034) and NIH R21 AA015077 to Evan D. Morris and from the Indiana Alcohol Research Center at Indiana University (P60 AA07611-17, P44) to David A Kareken. We acknowledge the support of the General Clinical Research Center at the Indiana University School of Medicine (M01 RR00750).

References

Bahn M M, Huang S C, Hawkins R A, Satyamurthy N, Hoffman J M, Barrio J R, Mazziotta J C and Phelps M E 1989 Models for in vivo kinetic interactions of dopamine D2-neuroreceptors and 3-(2'-[18F]fluoroethyl)spiperone examined with positron emission tomography *J. Cereb. Blood Flow Metab.* **9** 840–9

Christian B T, Narayanan T, Shi B, Morris E D, Mantil J and Mukherjee J 2004 Measuring the in vivo binding parameters of [18F]-fallypride in monkeys using a PET multiple-injection protocol *J. Cereb. Blood Flow Metab.* **24** 309–22

Constantinescu C C, Bouman C and Morris E D 2007 Nonparametric extraction of transient changes in neurotransmitter concentration from dynamic PET data *IEEE Trans. Med. Imaging* **26** 359–73

Eckernas S A, Aquilonius S M, Hartvig P, Hagglund J, Lundqvist H, Nagren K and Langstrom B 1987 Positron emission tomography (PET) in the study of dopamine receptors in the primate brain: evaluation of a kinetic model using 11C-N-methyl-spiperone *Acta Neurol. Scand.* **75** 168–78

Endres C J and Carson R E 1998 Assessment of dynamic neurotransmitter changes with bolus or infusion delivery of neuroreceptor ligands *J. Cereb. Blood Flow Metab.* **18** 1196–210

Fisher R E, Morris E D, Alpert N M and Fischman A J 1995 *In vivo* imaging of neuromodulatory synaptic transmission using PET: a review of relevant neurophysiology *Human Brain Mapping* 24–34

Innis R B *et al* 2007 Consensus nomenclature for in vivo imaging of reversibly-binding radioligands *J. Cereb. Blood Flow Metab.*

Kareken D, Constantinescu C, Morris E D, Cheng T, O'Connor S and Yoder K K 2007 Effects of alcohol-related cues and alcohol infusion on striatal dopamine: An [11C]raclopride PET study in humans with parametric analysis [abstract] *Res. Soc. Alcohol.*

Kendall M G 1955 *Rank Correlation Methods* (New York: Hafner Publishing Co.)

Logan J, Fowler J S, Volkow N D, Wang G J, Ding Y S and Alexoff D L 1996 Distribution volume ratios without blood sampling from graphical analysis of PET data *J. Cereb. Blood Flow Metab.* **16** 834–40

Mirenowicz J and Schultz W 1994 Importance of unpredictability for reward responses in primate dopamine neurons *J. Neurophysiol.* **72** 1024–7

Morris E D, Fisher R E, Alpert N M, Rauch S L and Fischman A J 1995 In vivo imaging of neuromodulation using positron emission tomography: optimal ligand characteristics and task length for detection of activation *Human Brain Mapping* 35–55

Morris E D and Yoder K K 2007 Positron emission tomography displacement sensitivity: predicting binding potential change for positron emission tomography tracers based on their kinetic characteristics *J. Cereb. Blood Flow Metab.* **27** 606–17

Morris E D, Yoder K K, Wang C, Normandin M D, Zheng Q H, Mock B, Muzic R F Jr and Froehlich J C 2005 ntPET: a new application of PET imaging for characterizing the kinetics of endogenous neurotransmitter release *Mol. Imaging* **4** 473–89

Olsson H and Farde L 2001 Potentials and pitfalls using high affinity radioligands in PET and SPET determinations on regional drug induced D2 receptor occupancy–a simulation study based on experimental data *Neuroimage* **14** 936–45

Pan W X, Schmidt R, Wickens J R and Hyland B I 2005 Dopamine cells respond to predicted events during classical conditioning: evidence for eligibility traces in the reward-learning network *J. Neurosci.* **25** 6235–42

Pappata S, Dehaene S, Poline J B, Gregoire M C, Jobert A, Delforge J, Frouin V, Bottlaender M, Dolle F, Di Giamberardino L and Syrota A 2002 In vivo detection of striatal dopamine release during reward: a PET study with [(11)C]raclopride and a single dynamic scan approach *Neuroimage* **16** 1015–27

Ramchandani V A, O'Connor S, Blekher T, Kareken D, Morzorati S, Nurnberger J Jr and Li T K 1999 A preliminary study of acute responses to clamped alcohol concentration and family history of alcoholism 11 *Alcohol Clin. Exp. Res.* **23** 1320–30

Schultz W, Tremblay L and Hollerman J R 2000 Reward processing in primate orbitofrontal cortex and basal ganglia *Cereb. Cortex* **10** 272–84

Yoder K K, Wang C and Morris E D 2004 Change in binding potential as a quantitative index of neurotransmitter release is highly sensitive to relative timing and kinetics of the tracer and the endogenous ligand *J. Nucl. Med.* **45** 903–11